Pharmacologic Characterization of a Potent Inhibitor of Class I Phosphatidylinositide 3-Kinases

Florence I. Raynaud,[1] Suzanne Eccles,[1] Paul A. Clarke,[1] Angela Hayes,[1] Bernard Nutley,[1] Sonia Alix,[1] Alan Henley,[1] Francesca Di-Stefano,[1] Zahida Ahmad,[1] Sandrine Guillard,[1] Lynn M. Bjerke,[1] Lloyd Kelland,[1] Melanie Valenti,[1] Lisa Patterson,[1] Sharon Gowan,[1] Alexis de Haven Brandon,[1] Masahiko Hayakawa,[2] Hiroyuki Kaizawa,[2] Tomonubu Koizumi,[2] Takahide Ohishi,[2] Sonal Patel,[3] Nahid Saghir,[3] Peter Parker,[4] Mike Waterfield,[5] and Paul Workman[1]

[1]Cancer Research UK Centre for Cancer Therapeutics, The Institute of Cancer Research, Haddow and McElwain Laboratories, Sutton, Surrey, United Kingdom; [2]Astellas Pharma, Inc., Drug Discovery Research, Tsukuba, Ibaraki, Japan; [3]PIramed Ltd., Slough, Berkshire, United Kingdom; [4]Cancer Research UK, London Research Institute, Lincoln's Inn Fields Laboratories; and [5]Ludwig Institute for Cancer Research, Department of Biochemistry and Molecular Biology, University College London, London, United Kingdom

Abstract

Extensive evidence implicates activation of the lipid phosphatidylinositide 3-kinase (PI3K) pathway in the genesis and progression of various human cancers. PI3K inhibitors thus have considerable potential as molecular cancer therapeutics. Here, we detail the pharmacologic properties of a prototype of a new series of inhibitors of class I PI3K. PI103 is a potent inhibitor with low IC_{50} values against recombinant PI3K isoforms p110α (2 nmol/L), p110β (3 nmol/L), p110δ (3 nmol/L), and p110γ (15 nmol/L). PI103 also inhibited TORC1 by 83.9% at 0.5 μmol/L and exhibited an IC_{50} of 14 nmol/L against DNA-PK. A high degree of selectivity for the PI3K family was shown by the lack of activity of PI103 in a panel of 70 protein kinases. PI103 potently inhibited proliferation and invasion of a wide variety of human cancer cells *in vitro* and showed biomarker modulation consistent with inhibition of PI3K signaling. PI103 was extensively metabolized, but distributed rapidly to tissues and tumors. This resulted in tumor growth delay in eight different human cancer xenograft models with various PI3K pathway abnormalities. Decreased phosphorylation of AKT was observed in U87MG gliomas, consistent with drug levels achieved. We also showed inhibition of invasion in orthotopic breast and ovarian cancer xenograft models and obtained evidence that PI103 has antiangiogenic potential. Despite its rapid *in vivo* metabolism, PI103 is a valuable tool compound for exploring the biological function of class I PI3K and importantly represents a lead for further optimization of this novel class of targeted molecular cancer therapeutic. [Cancer Res 2007;67(12):5840–50]

Introduction

The lipid kinase family of phosphatidylinositide 3-kinases (PI3K) are responsible for the generation of 3-phosphorylated inositides, including the important second messenger PtIns(3,4,5)P_3, resulting in activation of signal transduction pathways implicated in many physiologic processes (1–4). The class I enzymes, the most well characterized of the PI3K to date, are divided into class IA (p110α, p110β, and p110δ) and class IB (p110γ) according to their structure and interaction with p85 and p55 regulatory subunits (1, 5). Deregulation of the PI3K pathway has been reported in a significant proportion of cancers. For example, overexpression of p110α has been shown in ovarian, small cell lung, cervical, glioblastoma, head and neck, and bladder cancers (6–10). Activating mutations of the *PIK3CA* gene encoding p110α have been identified in a large number of cancers, including ovarian, breast, colon, and glioblastoma; in some cases, these were shown to be oncogenic (11–14). In addition to a role for p110α, recent studies have shown that oncogenic transformation can be induced by all other class I isoforms (15). An alternative form of pathway activation results from the mutation of *phosphatase and tensin homologue deleted on chromosome 10* (*PTEN*), the gene that encodes the phosphatase that dephosphorylates the 3-phosphoinositides. This is the second most frequently mutated tumor suppressor gene after *p53* (16). Downstream of the lipid phosphorylation step regulated by PI3K and PTEN, *AKT* is amplified and overexpressed in ovarian, breast, and pancreatic cancers (17, 18), and *TSC2* mutations inhibit the formation of the tumor suppression complex TSC1-2 (19). Upstream of PI3K, growth factor receptors are mutated, overexpressed, or activated in many cancers (20). Furthermore, there is accumulating evidence to implicate PI3K-regulated signaling in angiogenesis and metastasis (21–24). Altogether, the frequency of deregulation of this pathway suggests that the lipid kinases that produce PtIns(3,4,5)P_3 are attractive targets for cancer drug discovery (25). A number of chemical inhibitors of the PI3K family have been developed, but these either lack potency or specificity or exhibit unsuitable pharmaceutical properties (26). The most frequently used inhibitors to date are the natural product wortmannin and the flavone LY294002. Recently, however, more drug-like inhibitors have been described. PWT-458 is a pegylated derivative of wortmannin, an unstable and broad-spectrum natural product PI3K inhibitor, that has been shown to suppress growth of U87MG glioma *in vitro* and *in vivo* with a concomitant decrease in phosphorylation of AKT (27). A series of semisynthetic derivatives of the natural product viridins have also been described, of which PX-866 has shown antitumor

Note: Supplementary data for this article are available at Cancer Research Online (http://cancerres.aacrjournals.org/).

P. Workman is a Cancer Research UK Life Fellow.

S. Guillard and L. Bjerke were recipients of studentships from The Institute of Cancer Research.

Current address for B. Nutley: Cantest Ltd., 4606 Canada Way, Bunaby, British Columbia, V5G1K5, Canada.

Current address for L. Kelland: Cancer Research Technology, Wolfson Institute for Biomedical Research, University College London, Gower Street, London CE1 6BT, United Kingdom.

Requests for reprints: Florence I. Raynaud, Cancer Research UK Centre for Cancer Therapeutics, The Institute of Cancer Research, Brookes Lawley Building, 15 Cotswold Road, Sutton, Surrey, United Kingdom, SM2 5NG. Phone: 44-2087224212; E-mail: Florence.Raynaud@icr.ac.uk and Paul Workman, Cancer Research UK Centre for Cancer Therapeutics, The Institute of Cancer Research, Brookes Lawley Building, 15 Cotswold Road, Sutton, Surrey, United Kingdom. E-mail: Paul.Workman@icr.ac.uk.

doi:10.1158/0008-5472.CAN-06-4615

efficacy in A549 lung carcinoma and OVCAR-3 ovarian carcinoma xenografts and also potentiated the effects of gefitinib (28, 29). A triazine derivative, ZSTK474, was described as a potent PI3K inhibitor with antitumor activity in A549 lung adenocarcinoma, PC3 prostate adenocarcinoma, and WiDr colorectal carcinoma xenografts following oral administration (30).

We previously reported the discovery of three new series of PI3K inhibitors (31–33). Here, we describe the detailed pharmacologic properties of a novel synthetic small molecule of the pyridofuropyrimidine class, PI103, which is a potent and selective inhibitor of class I PI3K (31). Inhibition of human cancer cell growth *in vitro* by PI103 is associated with pharmacodynamic biomarker effects consistent with target inhibition. PI103 shows antitumor activity *in vivo* in several human tumor xenograft models, including cancers with documented abnormalities in the PI3K pathway, in which pharmacodynamic effects were also observed. In addition, PI103 inhibits tumor cell invasion both *in vitro* and *in vivo* and also blocks endothelial cell function and vascularization of human tumor xenografts. As this study was being completed, PI103 was also shown in a chemical biology and screening approach to exhibit selective inhibition of the PI3K pathway and to inhibit proliferation of human glioma cells (34–36). PI103 represents an exploratory compound for investigating the therapeutic relevance of PI3K inhibitors in cancers with a variety of genetic aberrations in the pathway and is a lead for further optimization of a novel class of targeted molecular cancer therapeutic.

Materials and Methods

Compound supply. PI103 was synthesized originally at Astellas Pharmaceuticals (32). Recent batches were provided by PIramed Ltd. All batches had similar potency and selectivity.

Enzyme assays. Enzyme assays were done using human recombinant enzymes. A scintillation proximity radiometric assay was done in the presence of 1 μmol/L ATP (31, 32). IC_{50} values were determined by fitting a sigmoidal dose-response and represent means of three experiments. The selectivity against a panel of 70 kinases was assessed at a concentration of 10 μmol/L (Upstate).

Cell culture. The human cell lines U87MG, HCT116, HT29, PC-3, MDA-MB-468, MDA-MB-435, A549, SKOV-3, MDA-MB-435, IGROV-1, OVCAR-3, and Detroit 562 were obtained from the American Type Culture Collection. A2780 cells were obtained from the European Collection of Cell Cultures. All cell lines were grown in DMEM (Invitrogen Ltd.) containing 2 mmol/L glutamine (Life Technologies) with 100 units/mL penicillin and 100 μg/mL streptomycin (Life Technologies) and supplemented with 10% fetal bovine serum (PAA) in 5% CO_2 in air at 37°C. Human umbilical vein endothelial cells (pooled HUVEC) and their appropriate growth medium and supplements were obtained from TCS CellWorks. Cells were cultured according to the supplier's instructions and used at passages 3 to 8. Cell viability was routinely greater than 90%, as judged by trypan blue exclusion. All cell lines routinely tested negative for *Mycoplasma* by PCR. The GI_{50} values were determined using a sulfurhodamine blue assay following 96 h of continuous exposure (37).

Immunoblotting and immunoassay. Cells were treated with 1× or 5× GI_{50} PI103 for various times, and protein extracts were prepared by washing the cells once in ice-cold PBS and then lysing with cell lysis buffer (Cell Signaling Technologies), supplemented with protease inhibitors (Boehringer/Roche). Determination of protein concentration was done using BCA Protein Assay kit (Pierce). Tumors were snap frozen using liquid nitrogen immediately following excision and stored at −80°C until processed. They were homogenized into a fine power under liquid nitrogen using a model 6750 freezer mill (Glen Crestor). Ground powder was immediately resuspended in lysis buffer [150 mmol/L NaCl, 1 mmol/L EDTA, 50 mmol/L Tris (pH 7.4), 1% (v/v) Triton X-100, 1 mmol/L NaF, 1 mmol/L sodium orthovanadate, 10 mg/mL TLCK, 5 μmol/L fenvalerate, 5 μmol/L bpVphen, 1 mmol/L phenylmethylsulfonyl fluoride, protease cocktail (1:100), phosphatase cocktail I and II (1:50)] by aspirating through a 23-gauge needle. Samples were incubated on ice and centrifuged at 1,500 × *g* for 10 min, and the supernatants were recovered and aliquoted.

Equal amounts of protein were separated by electrophoresis through NuPage Bis-Tris 4% to 12% gradient gels (Invitrogen); proteins were transferred onto nitrocellulose or polyvinylidene difluoride (0.45 μm) pore membranes using the NuPage system and protocol from Invitrogen. Antibodies were obtained from the following suppliers: phosphorylated AKT (p-AKT) Ser^{473}, p-AKT Thr^{308}, p-GSK3β Ser^{9}, GSK3β, cleaved poly(ADP-ribose) polymerase (PARP; Cell Signaling Technologies), cyclin D1 (NeoMarkers), glyceraldehyde-3-phosphate dehydrogenase (Chemicon International). All antibodies were used as recommended by the manufacturer, and specific antigen-antibody interaction was detected with a horseradish peroxidase–conjugated secondary antibody IgG using enhanced chemiluminescence Western blotting detection reagents (Amersham Biosciences).

Electrochemiluminescent immunoassay. A Meso Scale Discovery system was used to measure the levels of AKT activation in tumors following exposure to PI103. Multi-spot p-AKT Ser^{473}/total AKT assays were performed with 10 μg protein in duplicate. The protocol used was as recommended by the manufacturer except that samples were incubated on the plates overnight before addition of secondary antibody.

Flow cytometry. DNA histograms were generated by flow cytometry analysis. Cells were washed in PBS and fixed in 70% ethanol for 30 min at 4°C. Fixed cells were washed once with PBS, resuspended in PBS containing 100 mg/mL RNase A and 40 mg/mL propidium iodide, and incubated for 30 min at 37°C. All samples were analyzed on a Beckman Coulter EPICS Elite ESP flow cytometer. Data were analyzed, and histograms were plotted using winMDI version 2.5 flow cytometry application software (Scripps Institute).

Measurement of caspase activation. Activation of apoptotic effector caspases that cleave the DEVD (Asp-Glu-Val-Asp) motif was assayed using a non-fluorescent caspase substrate Z-DEVD-R110 that releases fluorescent rhodamine-110 when cleaved by caspases that recognise the DEVD motif. Briefly, cells were seeded at 4,000 per well in a 96-well plate and treated 24 h later with inhibitors or vehicle control for 1 to 3 days. Caspase activity was assessed by adding an equal volume of reagent and substrate (Promega), incubating for 16 h, and measuring rhodamine-110 fluorescence at 535 nm following excitation at 485 nm using a Victor 1420 plate reader (Perkin-Elmer).

Localization assays. Redistribution assays of green fluorescent protein (GFP)–tagged proteins were done at Bioimage.[6] Briefly, the effects of the inhibitors on cellular translocation of FKHR, AKT1, AKT2, AKT3, and PDK1 were compared with those of wortmannin. The FKHR redistribution assay was done in U2OS cells cultured with 0.7% serum, and all other assays were done in Chinese hamster ovary (CHO) cells in 0.05% serum with 0.1% bovine serum albumin following stimulation with 100 nmol/L insulin-like growth factor-1 (IGF-1). Fluorescence was monitored with an In-Cell Analyser (Amersham). Concentration-response curves were derived from Prism 3.02 (GraphPad), and IC_{50} values were determined. Z' factors were above 0.5.

Pharmacokinetics and metabolism. Microsomes (mouse or human) were obtained from Tebu-Bio and incubated for 30 min with 1 or 10 μmol/L inhibitor as described (38). All animal experiments were done in accordance with local requirements for animal experimentation and national United Kingdom Co-ordinating Committee on Cancer Research guidelines (39). Female BALB/c mice (6–8 weeks old; Charles River) were dosed i.v. with 2.5 mg/kg PI103 in 10% DMSO, 0.5% Tween 20 in saline, or 50 mg/kg PI103 in 20% 4-hydroxypropyl β-cyclodextrin in saline at 0.1 mL/10 g i.p. Blood was collected after serial bleeding and centrifuged, and the plasma was frozen at −80° C. Tissues were snap frozen in dry ice and kept at −80°C until analysis.

[6] http://www.bioimage.com

Quantitative analysis was done by liquid chromatography tandem mass spectrometry (LC-MS/MS) using multiple reaction monitoring on a ThermoFinnigan TSQ 700 equipped with an electrospray ionization source. Chromatographic separation was achieved by a Waters system (Wisp 717 autosampler and 600 MS pump and gradient former) on a Discovery C18 column (Sigma-Aldrich; 5 cm × 4.6 mm inner diameter) with a 4-min 20 to 100 linear gradient of methanol in 0.1% formic acid following a 3-min isocratic period at 0.6 mL/min. The following transitions were monitored (341.9 > 261.9 at −35 V, 554 > 362 at −40 V). Quantitation was done versus external calibration at the level of 2 to 20,000 nmol/L (8 points). Quality controls were included at concentrations of 15, 750, and 5,000 nmol/L. Aliquots (100 μL) of mouse plasma were added to 10 μL of internal standard (an analogue of PI103, used at concentrations of 5,000 nmol/L) and precipitated with 3 volumes of methanol. Following centrifugation at 2,500 × *g* for 5 min, 20 μL supernatant was analyzed. Tissues were homogenized in 2 or 3 volumes PBS and treated as plasma. Quantitation was done on Excalibur software. The assay was linear over the range of concentrations analyzed ($r > 0.99$).

Qualitative measurements (metabolite detection and characterization) were done by LC-MS/MS on a Thermoseparation AS3000 autosampler, P4000 quaternary pump, and UV1000 detector attached to a LCQ ion trap (ThermoFinnigan). Samples were separated using the same column as above with a slower gradient of 10% to 90% methanol over 6 min after 0.5-min isocratic at 1 mL/min. The scan range was 50 to 1,000 amu. Pharmacokinetic calculations were done using WinNonlin noncompartmental analysis model 201 for plasma following i.v. administration and model 200 for tissues and plasma following i.p. administration (40).

Human tumor xenograft efficacy and pharmacodynamic studies. For s.c. tumor xenograft models, 2×10^6 cells were injected s.c., bilaterally, into female (or in the case of PC3 prostate tumors, male) NCr athymic mice 6 to 8 weeks of age, bred in-house. The breast carcinomas were inoculated into mammary fat pads. Dosing commenced when tumors were established (~5 mm mean diameter) for the period indicated. PI103 was prepared in 20% 4-hydroxypropyl β-cyclodextrin and injected i.p. Tumors were measured across two perpendicular diameters, and volumes were obtained from the following formula: $V = 4/3\pi\ [(d_1 + d_2)\ /\ 4]^3$ (41).

When the experiment was terminated, mice were bled, plasma samples were prepared, and tumors were excised and weighed; % treated/control (T/C) values were calculated from final tumor weights or, in the case of HCT116 carcinoma, from tumor volumes on the last day of therapy because tumors were allowed to grow out to observe recovery. Tumor samples were snap frozen for pharmacokinetic or pharmacodynamic analysis and, in some cases, cryopreserved or fixed for histologic examination. In the latter case, samples were sectioned and stained with H&E using standard techniques. For examination of vasculature, tumors were stained with rat anti-mouse endothelial antibody MECA 32 with goat anti-rat horseradish peroxidase–conjugated secondary antibody as previously described (42).

OVCAR-3 ovarian cancer cells were passaged *in vivo*, and 5×10^6 cells were injected i.p. into female Ncr nu mice. Therapy commenced 15 days later and continued daily until day 30. Mice were sacrificed 15 min, and 4 h after the last drug dose, tumor burden was calculated, and samples taken for pharmacodynamic analysis by Western blotting. Visceral organs were examined for evidence of tumor invasion both macroscopically and by histology. In separate pharmacodynamic studies, mice bearing established OVCAR-3 orthotopic ascites tumors or s.c. U87MG glioblastoma xenografts were given two doses of 100 mg/kg PI103 in β-cyclodextrin vehicle i.p. before harvesting of tumor samples for p-AKT electrochemiluminescent immunoassay analysis at intervals after the final dose.

Cell migration and invasion assays. Cells were labeled by incubation with the green fluorescent dye Celltracker green 5-chloromethylfluorescein diacetate (Invitrogen) at 1 μmol/L for 1 h. Cells (2×10^4 in 350 μL serum-free media) were then placed into the upper well of an 8-μm pore Fluoroblok membrane insert in 24-well companion plates (BD Biosciences) in DMEM vehicle or various concentrations of PI103. Medium (800 μL) containing 5% heat-inactivated FCS was added to the lower chamber as a chemoattractant. The assay plates were incubated at 37°C in 5% CO_2 for 16 to 24 h (tumor cells) or 4 h (HUVEC). An inverted fluorescent microscope and digital camera (Olympus LX70) were used to obtain images of the migrated cells on the underside of the membrane. Three different fields of view were scored for each well. The number of migrated cells was calculated using Image Pro-Plus 4.0 software (Media Cybernetics). Invasion was assayed in a similar fashion using inserts coated with Matrigel. The observation period was extended to 36 h for tumor cells and 18 h for HUVEC.

Results

PI103 is a selective class I PI3K inhibitor. PI103 was synthesized following a high-throughput screen to identify inhibitors of the enzymatic activity of recombinant PI3K p110α (32). PI103 potently and competitively inhibited all class IA isoforms, α, β, and δ, with IC_{50} values of 2, 3, and 3 nmol/L, respectively. It is ~200-fold more potent than the commonly used broad-spectrum PI3K inhibitor LY294002 (IC_{50} = 500, 580, and 600 nmol/L against p110α, p110β, and p110δ, respectively). PI103 exhibited 5- to 7-fold less activity against the class IB p110γ isoform (IC_{50} = 15 nmol/L) and DNA-PK (IC_{50} = 14 nmol/L), a member of the PI3K superfamily, as well as 15- to 20-fold less activity against the class II PI3K C2β (IC_{50} = 43 nmol/L). In addition, there was at least 1,300-fold selectivity over the class III PI3K Vsp34 (IC_{50} = 3,950 nmol/L). PI103 inhibited TORC1 (83.9% inhibition at 0.5 μmol/L), consistent with recent data (33). There was no inhibition of PKCα or PKA at concentrations of 1 μmol/L. PI103 was also screened against a panel of 70 protein kinases that are representative of the human kinome and containing a number of oncogenic proteins such as cyclin-dependent kinases, receptor tyrosine kinases, and kinases involved in the regulation of signal transduction, including AKT. Little or no inhibitory activity was seen at 10 μmol/L PI103, indicating a high degree of selectivity for the PI3K superfamily (data not shown).

PI103 inhibits the PI3K pathway and proliferation of cancer cells *in vitro*. Figure 1*A* shows the cellular GI_{50} values of PI103, evaluated in a panel of human cancer cell lines comprising prostate, lung, ovary, colon, and breast cancer, glioblastoma, and oropharyngeal carcinoma and following 96 h of continuous treatment with PI103. These cell lines have different genetic abnormalities that can result in activation of the PI3K pathway (e.g., PTEN deletion or a PI3K p110α mutation within the kinase or other regulatory domains; refs. 11, 13, 43–46). PI103 exhibited a range of GI_{50} values from 0.06 to 0.93 μmol/L compared with 4.60 to 12.10 μmol/L for LY294002. Thus, the greater potency of PI103 on the molecular target was also carried over into enhanced growth inhibition in cancer cells. PI103 showed activity in cell lines with wild-type and mutant PTEN and retained potency in cells with mutant *PIK3CA.* These included the Detroit 562 oropharyngeal carcinoma cell line that harbors the mutant *PIK3CA* H1047R, the HCT116 colorectal carcinoma line with an H1047R mutation in the kinase domain, the A2780 ovarian carcinoma line with a C2 domain mutation, and the IGROV-1 ovarian carcinoma with a p85 binding domain mutation and stop 1069W mutation resulting in extension of the protein by four amino acids (A2780 and IGROV; data not shown; ref. 11).

Similar to LY294002, treatment with PI103 resulted in a time- and concentration-dependent decrease in phosphorylation of AKT Ser^{473} in all cell lines (Fig. 1*A* and *B*; Supplementary Fig. S1*A* and *B*). Figure 1*B* shows decreased phosphorylation of AKT Ser^{473} following treatment of HCT116 human colorectal carcinoma cells with increasing PI103 (1–10× GI_{50}) or of U87MG glioblastoma and PC3 prostate cancer cells (1× and 5× GI_{50}; Supplementary Fig. S1*A*

A

Cell line	Molecular features	LY294002 GI_{50}	PI103 GI_{50}
PC3	PTEN null	4.60 ± 0.50	0.10 ± 0.02
MDA–MB–468	PTEN null	6.50 ± 1.12	0.69 ± 0.31
U87MG	PTEN null	9.80 ± 0.83	0.18 ± 0.02
HCT116	PIK3CA mutant	10.50 ± 0.35	0.93 ± 0.05
Detroit 562	PIK3CA mutant	12.10 ± 2.27	0.36 ± 0.02
IGROV-1	PIK3CA mutant, PTEN mutant	5.50 ± 1.67	0.06 ± 0.04
A2780	PIK3CA mutant, PTEN mutant	5.58 ± 0.68	0.50 ± 0.07
MDA–MB–435	Activated AKT	15.28 ± 2.85	0.13 ± 0.10
A549	Activated AKT	9.00 ± 0.34	0.21 ± 0.09

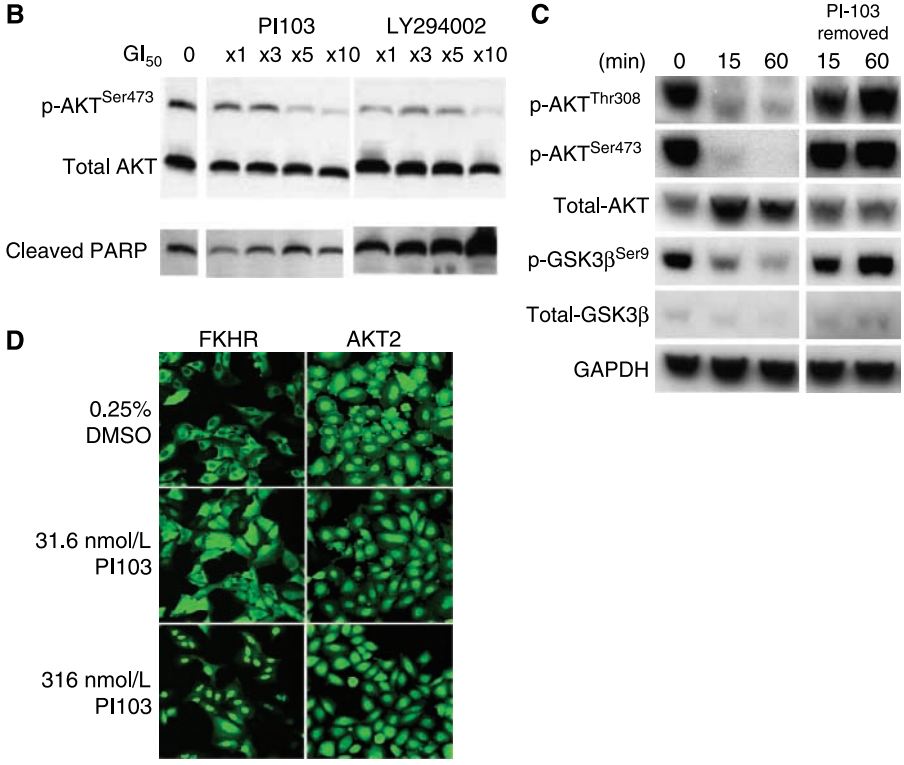

Figure 1. Molecular and cellular effects of PI103 on cancer cells *in vitro*. *A,* effects on cellular proliferation as assessed by the sulfurhodamine B assay in 96-well plate format. Mean ± SD of three independent determinations of GI_{50} (μmol/L) following 96 h of continuous exposure to compound. The cell lines presented exhibit a variety of mechanisms of deregulation of the PI3K pathway (PC3, U87MG, MDA-MB-468 are PTEN null; A2780 has a homK128-R130 deletion in PTEN and a C2 domain hetE365K mutation of p110α; IGROV-1 has a hetT319F deletion and frameshift in PTEN, a p85 binding domain hetR38C mutation of p110α and an additional hetX1069W mutation that extends the COOH terminus of p110α by four amino acids; HCT116 and Detroit 562 have a hetH1047R mutation of the p110α kinase domain; MDA-MB-435 and A549 have high levels of p-AKT). *B,* immunoblot analysis of HCT116 cells treated with 1, 2.5, 5, and 10× GI_{50} PI103 or LY294002 for 24 h. *C,* immunoblot analysis of U87MG cells treated with 5× GI_{50} concentration of PI103 for 2 h. Cells were then washed in PBS and cultured in PI103-free medium. Samples were analyzed after 15 and 60 min of exposure and 15 and 60 min after removal of PI103 and addition of PI103-free medium. Note: a batch of total AKT antibody was found to preferentially recognized the unphosphorylated form relative to the phosphorylated form. Glyceraldehyde-3-phosphate dehydrogenase (*GAPDH*) was used as the loading control. *D,* PI103 treatment before IGF-1 stimulation of U2OS cells expressing a GF-FKHR fusion protein inhibits phosphorylation of FKHR-GFP resulting in its nuclear accumulation (*left*). PI103 treatment of CHO cells expressing a GFP-AKT2 fusion protein blocks distribution of AKT2 to the plasma membrane following IGF-1 stimulation (*right*).

and *B*). The effects of PI103 on the downstream components of the PI3K pathway were rapid, with inhibition of phosphorylation of AKT Ser^{473} and Thr^{308} and GSK3β Ser^{9} occurring within 15 min of treatment (Fig. 1*C*). This was followed by an equally rapid recovery 15 min after PI103 was removed and the cells were transferred to drug-free medium.

The effects of PI103 on the redistribution of a forkhead transcription factor (FKHR), PDK1, AKT1, AKT2, or AKT3 following stimulation with IGF-1 were measured in U20S human osteosarcoma cells expressing FKHR fused to GFP or CHO cells expressing PDK1, AKT1, AKT2, and AKT3 fused to GFP. Activation of PI3K and production of PIP_3 result in recruitment of PDK1 and AKT to the plasma membrane via their PH domains (45). Activated AKT subsequently phosphorylates a number of substrates (including FKHR) that prevents their translocation from the cytoplasm to the nucleus (46). Consistent with inhibition of PI3K signaling, PI103 induced the redistribution of GFP-tagged FKHR from the cytoplasm to the nucleus (IC_{50} = 30 nmol/L) in U2OS cells (Fig. 1*D, left*) and inhibited the localization of GFP-AKT1, GFP-AKT2, GFP-AKT3 and GFP-PDK1 to the plasma membrane in CHO cells with IC_{50} values of 17, 13, 11, and 66 nmol/L respectively (Fig. 1*D, right*, AKT2; Supplementary Fig. S1*C*). PI103 had a similar potency to wortmannin in all of these assays; in contrast, LY294002 was less potent, with 200-fold higher IC_{50} values (data not shown).

PI103 also decreased cyclin D1 expression as early as 4 h post treatment in U87MG cells (Fig. 2*A*). This was consistent with a time- and concentration-dependent G_1 cell cycle arrest that was detected by flow cytometry in all the cell lines listed in Fig. 1*A*. Figure 2*B* and *C* illustrate typical cell cycle data for U87MG glioblastoma cells. Note that there was no evidence for a sub-G_1 peak associated with the induction of apoptotic cell death in U87MG cells (Fig. 2*C*) or any other of the cell lines listed in Fig. 1*A* (data not shown). The similar molecular signature and cell cycle effects of PI103 in PC3 cells are presented as supplemental data (Supplementary Fig. S1*D*). Treatment of the same human cancer cell line panel with LY294002 at 5× and 10× GI_{50} concentrations frequently resulted in apoptosis as detected by cleavage of PARP, a caspase substrate. However, similar increases in PARP cleavage

were not apparent following PI103 treatment (Fig. 1*B*). The induction of apoptosis by LY294002, but not PI103, was confirmed in HCT116 cells by direct measurement of the activation of the apoptotic effector proteases (caspases) following 1 to 3 days of exposure of up to 10× GI_{50} (Fig. 2*D*).

Pharmacokinetics and metabolism of PI103. PI103 was metabolized by >70% after 30 min of incubation with human and mouse microsomes under standard conditions (Fig. 3*A*). The main metabolite was the glucuronide of PI103 formed on the phenol ring, representing on average 57% of the total metabolites. In addition, a hydroxylated product on the morpholino moiety and a hydroxylated glucuronide were also formed. This resulted in opening of the morpholino ring, which we observed previously with LY294002 and other benzochromenone DNA-PK inhibitors (47, 48).

The concentration versus time curves in plasma, liver, kidney, and spleen following 2.5 mg/kg PI103 given i.v. to female BALB/C mice are shown in Fig. 4*B*. Pharmacokinetics of PI103 showed a high volume of distribution at steady state (V_{ss} = 0.0516 L). This was consistent with a very rapid tissue distribution, resulting in C_{max} occurring 5 min after dosing in liver, kidney, and spleen (Fig. 3*B*). The liver to plasma ratio was 1.3 versus 0.7 for kidney and spleen. The compound cleared from plasma with a rate of 0.19 L/h, which exceeds liver blood flow (Fig. 3*C*). Rapid tissue clearance was also seen.

Following i.p. administration of 50 mg/kg PI103, the apparent clearance was similar to that observed following i.v. dosing (0.12 L/h), but the concentrations were sustained in plasma and remained above GI_{50} levels for longer than 12 h (Fig. 3*D*). This contrasts with previous observations with LY294002, where plasma levels remained above active levels for only 1 h with comparable tissue distribution to that of PI103 (47). These encouraging results prompted us to investigate pharmacokinetic, pharmacodynamic, and efficacy effects in tumor-bearing animals.

Following 14 daily doses of 40 or 70 mg/kg PI103 i.p. in 20% 4-hydroxypropyl β-cyclodextrin to mice bearing U87MG glioblastoma xenografts, measurement of the peak area ratio of parent to glucuronide in both plasma and tissue showed extensive glucuronidation with 20-fold more glucuronide than parent compound in plasma (Fig. 4*A*). Despite this extensive metabolism, tumor levels of parent compound were found to be above GI_{50} levels for 2 h (Fig. 4*B*).

PI103 decreases AKT phosphorylation *in vivo*. Following two doses, 12 h apart, of 100 mg/kg PI103 i.p. in female Ncr nude mice bearing U87MG human glioblastoma xenografts, there was a reproducible and significant drop in phosphorylation of AKT on Ser^{473} 15 min to 2 h after dosing, consistent with inhibition of the PI3K pathway. The ratio of p-AKT Ser^{473}/total AKT measured by the electrochemiluminescent immunoassay reached a nadir at 30 to 60 min (falling to ~50% of control levels) and returned to control levels by 4 h (Fig. 4*C*). This is consistent with intratumoral levels of PI103 measured over the same period in this xenograft model (Fig. 4*B*).

Antitumor activity *in vivo*. Given the pharmacokinetic and pharmacodynamic data described above, we next sought evidence of therapeutic efficacy in human tumor xenografts selected for evidence of activation of the PI3K pathway by differing genetic events. As shown in Fig. 5, PI103 exhibited therapeutic activity at well-tolerated doses (<15% weight loss) in a number of human tumor models, including the PTEN null U87MG glioblastoma, PC3 prostate, and MDA-MB-468 breast carcinomas (Fig. 5*A* and *B*) and the *PIK3CA* mutant HCT 116 colon carcinoma (Fig. 5*C*). In the case of the HCT116 colon carcinoma, dosing was terminated on day 14 when the T/C, calculated from tumor volumes, was 68% and 28% for animals dosed once or twice daily with 30 mg/kg PI103, respectively. On day 21, when the experiment was terminated, the tumors in the former group had recovered to control values, but in the latter group, the T/C was still 48% (Fig. 5*D*).

In vivo efficacy of PI103 was also assessed in three further xenograft tumors. These were SKOV3 and IGROV-1 ovarian carcinomas that have p85 binding domain and kinase domain mutations of *PIK3CA*, respectively, as well as the MDA-MB-435 breast carcinoma that overexpresses ERB-B2 (Fig. 5*D*). Statistically

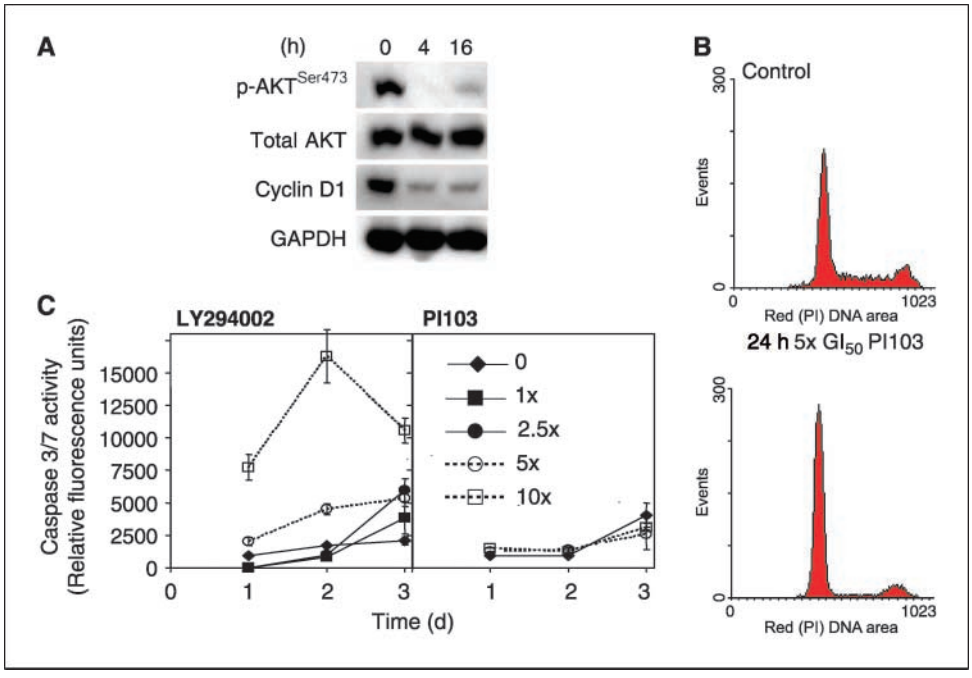

Figure 2. Effects of PI103 on cell cycle and apoptosis *in vitro*. *A,* immunoblot analysis of U87MG cells following treatment with 5× GI_{50} concentrations of PI103 for 4 and 16 h. Note the significant decrease in cyclin D1 expression appearing as early as 4 h posttreatment. *B, top,* cell cycle analysis by flow cytometry following 24 h of treatment of U87MG cells with vehicle only. Cells were labeled with propidium iodide (*PI*). *Bottom,* cell cycle effects observed following 24 h of treatment of U87MG cells with 5× GI_{50} concentration of PI103. Cells were labeled with propidium iodide and show a G_1 arrest with a decrease in S phase. *C,* activation of apoptotic effector caspases was measured in HCT116 cells 1 to 3 d following exposure to 1 to 10× GI_{50} LY294002 or 5 and 10× GI_{50} PI103.

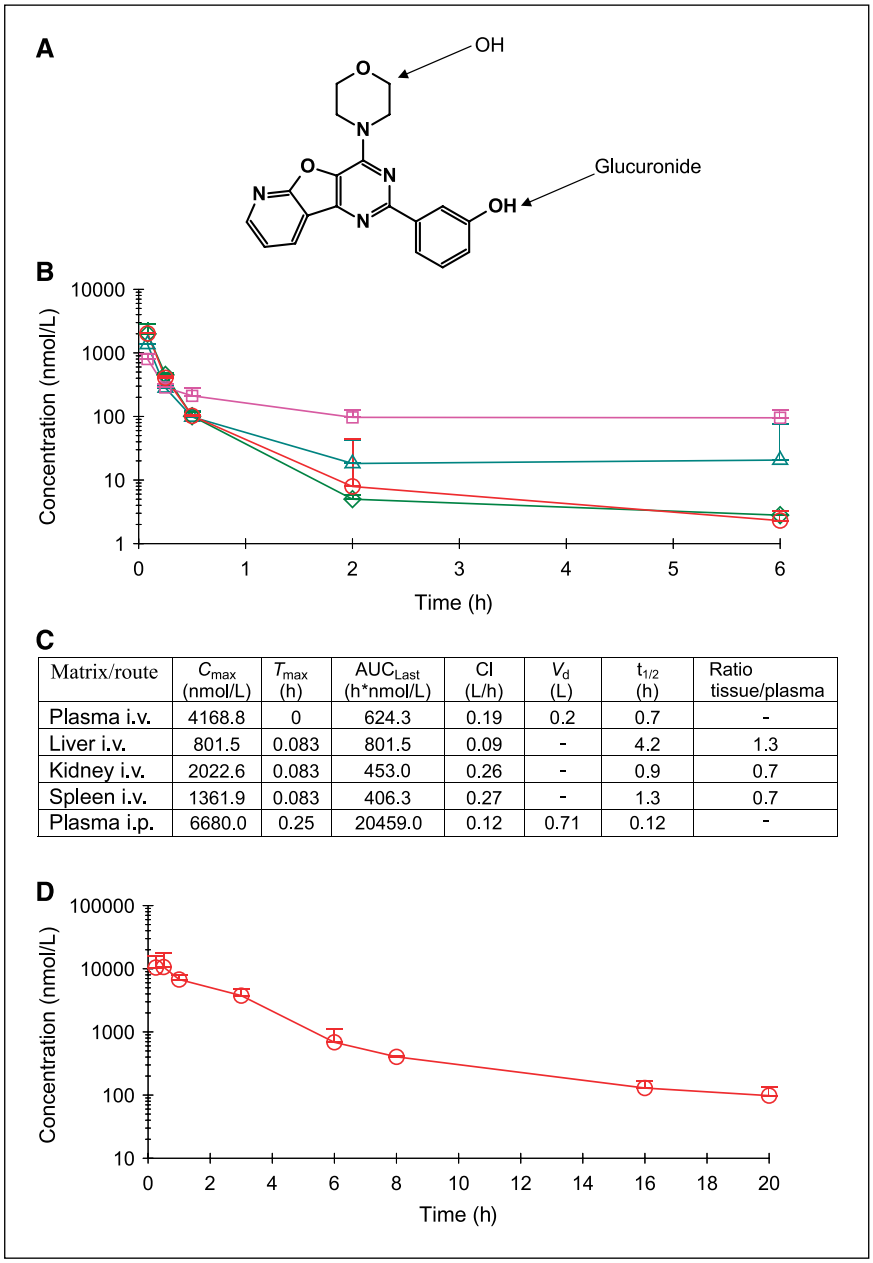

Matrix/route	C_{max} (nmol/L)	T_{max} (h)	AUC_{Last} (h*nmol/L)	Cl (L/h)	V_d (L)	$t_{1/2}$ (h)	Ratio tissue/plasma
Plasma i.v.	4168.8	0	624.3	0.19	0.2	0.7	-
Liver i.v.	801.5	0.083	801.5	0.09	-	4.2	1.3
Kidney i.v.	2022.6	0.083	453.0	0.26	-	0.9	0.7
Spleen i.v.	1361.9	0.083	406.3	0.27	-	1.3	0.7
Plasma i.p.	6680.0	0.25	20459.0	0.12	0.71	0.12	-

Figure 3. Pharmacokinetics and metabolism of PI103. *A,* structure and metabolism of PI103. *B,* plasma (○) and tissue (liver, □; kidney, ◇; spleen, △) concentration versus time profile following i.v. administration of 2.5 mg/kg PI103 to BALB/c mice. PI103 levels were measured by LC-MS/MS using multiple reaction monitoring. *C,* pharmacokinetic parameters for plasma and tissue following administration of 2.5 mg/kg PI103 i.v. and for plasma following 50 mg/kg PI103 to female BALB/c mice. Pharmacokinetic parameters are maximum concentration (C_{max}), time of maximum concentration (T_{max}), area under the concentration versus time curve (AUC), clearance (Cl), volume of distribution based on the terminal phase (V_d), half-life ($t_{1/2}$). *D,* plasma concentration versus time profile and pharmacokinetic parameters following 50 mg/kg PI103 administered i.p. to female BALB/c mice. PI103 levels were measured by LC-MS/MS by multiple reaction monitoring.

significant tumor efficacy ($P < 0.05$) was obtained in two of three of these experiments and overall in seven tumor models described in this section (Fig. 5*D*).

Inhibition of tumor cell and endothelial cell migration and invasion *in vitro* and *in vivo*. In a Transwell assay, PI103 inhibited chemomigration and invasion of a variety of tumor cells [e.g., HCT116 colon carcinoma, PC3 prostate carcinoma, MDA-MB-468 breast carcinoma, and Detroit 520 squamous cell carcinoma (Fig. 6*A*) and also U87MG glioblastoma (44% inhibition at 50 nmol/L, data not shown)]. HUVEC invasion of Matrigel was also significantly inhibited and to a greater extent than with LY294002 at equipotent concentrations based on proliferation GI_{50} (Fig. 6*B*).

Inhibition of invasion and angiogenesis were also observed in human breast tumor xenografts. Control tumors showed extensive invasion of underlying muscle and also of distended i.t. blood vessels (Fig. 6*C*, *top left* and *middle, arrows*), whereas tumors treated with 30 mg/kg PI103 twice daily remained encapsulated and noninvasive (Fig. 6*C, top right* and *middle*). In control tumors, there was an extensive vascular network, whereas in treated tumors, the vessels were fewer and smaller (Fig. 6*C, bottom*).

Finally, we tested the effects of PI103 in a xenograft model of late-stage ovarian carcinoma using i.p. implantation of OVCAR-3 cells. Therapy was initiated once tumors were well established and continued for 15 days. Daily doses of 15 mg/kg or 30 mg/kg, which are well below toxic levels, reduced tumor burden (T/C, 61–62%) in the peritoneal cavity (Supplementary Fig. S2*A*), and harvested tumor cells showed decreased levels of p-AKT Ser^{473} at 15 min and 4 h after dosing, although in the latter case, there was evidence of recovery of p-AKT Ser^{473} in one of the two samples (Supplementary Fig. S2*B*). We also noted a substantial decrease in i.p. tumor spread with undetectable liver, diaphragm, kidney, and ovary invasion and

reduced incidences of mesenteric and lymph node metastasis in PI103-treated animals, as assessed macroscopically and by histologic examination (Supplementary Fig. S2*C*). In a separate pharmacodynamic study, we showed inhibition of p-AKT Ser^{473} in OVCAR-3 ascites and solid tumor deposits measured by electrochemiluminescent immunoassay at 30 min and 2 h following two doses of 100 mg/kg PI103 (Supplementary Fig. S2*D*).

Discussion

In this study, we describe the detailed pharmacologic characterization of the pyridofuropyrimidine PI3K inhibitor PI103. We discovered this inhibitor by elaboration of a high-throughput screening hit (32). As also suggested in other recent reports, we find PI103 to be a highly potent inhibitor of PI3K (31, 34). We show here that PI103 exhibits a high degree of selectivity for class I PI3K versus a panel of 70 protein kinases. PI103 also inhibits DNA-PK and mammalian target of rapamycin (mTOR). In addition, we show the activity of PI103 in a range of tumors *in vitro* and in xenograft models, together with evidence of inhibition of invasion and angiogenesis.

PI103 is especially potent against the class IA enzymes α, β, and δ, with IC_{50} values of 2 to 3 nmol/L. The p110γ isoform is inhibited, with an IC_{50} of 15 nmol/L. This profile may be important therapeutically because all four class I enzymes have been shown to induce oncogenic transformation (15). It is valuable to have a potent and selective inhibitor to establish proof of concept for the effects of inhibition of a specific molecular target in cells. We have shown that the potency against PI3K translates well into cells, and that PI103 is very active in U87MG glioma and PC3 prostate carcinoma cells, both of which are PTEN null. In addition, PI103 was active both *in vitro* and *in vivo* in cells that harbor *PIK3CA* mutations in both kinase and regulatory domains (A2780, Detroit 562, HCT116, IGROV-1, and SKOV3). Such mutations have been

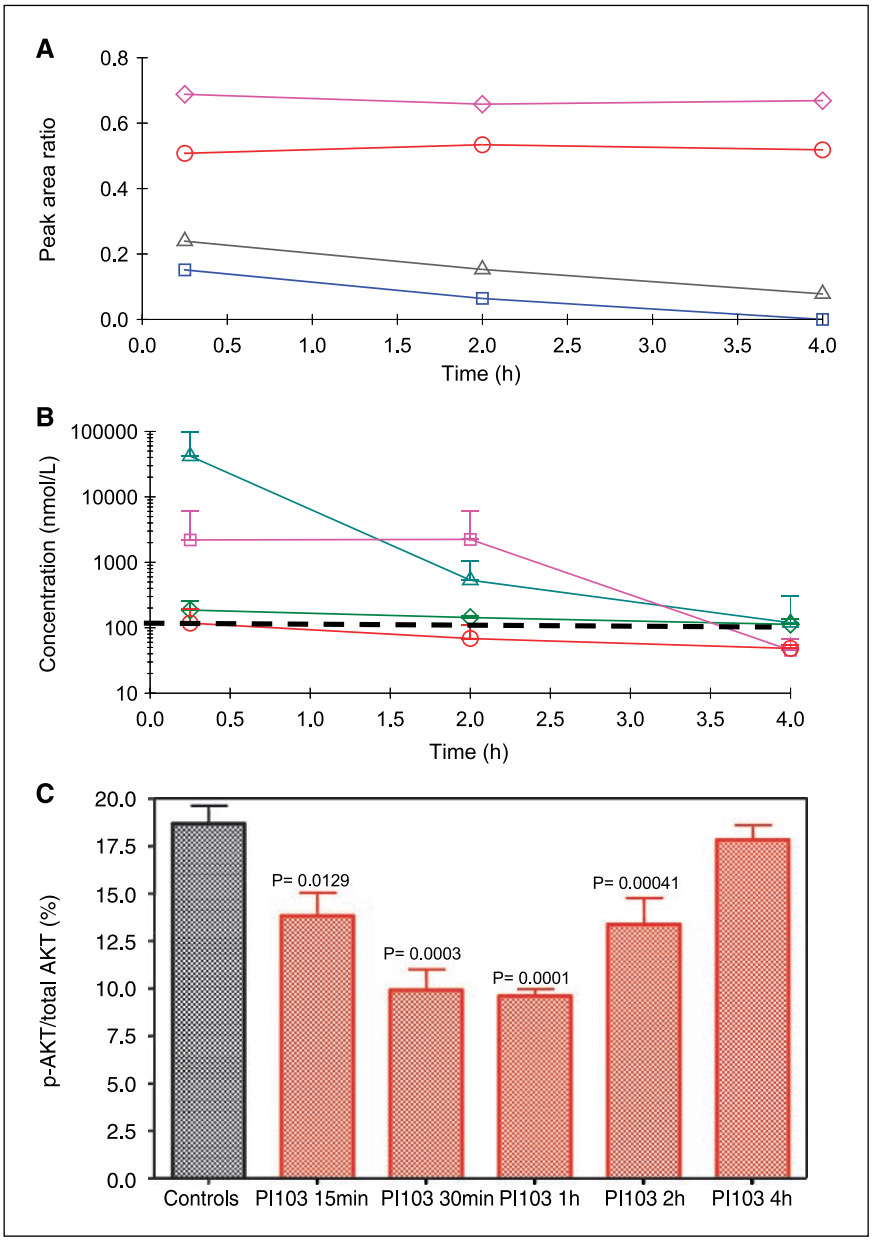

Figure 4. Pharmacokinetic-pharmacodynamic data for PI103 in NCr athymic mice bearing U87MG glioblastoma tumor xenografts. *A* and *B,* animals bearing U87MG tumor xenografts s.c. on the flank (~5 mm diameter) were given 40 or 70 mg/kg PI103 or an equivalent volume of vehicle (0.1 mL/10 g body weight) i.p. daily for 14 d as described in Materials and Methods. Plasma and tumor samples were collected 15 min, 2 h, and 4 h after the last dose. *A,* peak area ratios of PI103 (□, 40 mg/kg and △, 70 mg/kg) and glucuronide (○, 40 mg/kg and ◇, 70 mg/kg) in plasma. *B,* plasma (○, 40 mg/kg and ◇, 70 mg/kg) and tumor (□, 40 mg/kg and △, 70 mg/kg) levels of PI103. *Points,* means (n = 3); *bars,* SD. *Dashed line,* GI_{50}. *C,* pharmacodynamic effects. In a separate study, animals bearing U87MG xenografts (~8–10 mm diameter) were given two doses of 100 mg/kg PI103 or vehicle i.p. (evening of 1st day and morning of the 2nd day, 12 h apart). Tumor samples were collected from controls and treated animals at 15 min, 30 min, 1 h, 2 h, and 4 h after the second dose. Percentage of phosphorylation of AKT Ser^{473} was evaluated with the electrochemiluminescent immunoassay. *Columns,* means of ratio of p-AKT/total AKT (n = 3 tumors); *bars,* SD.

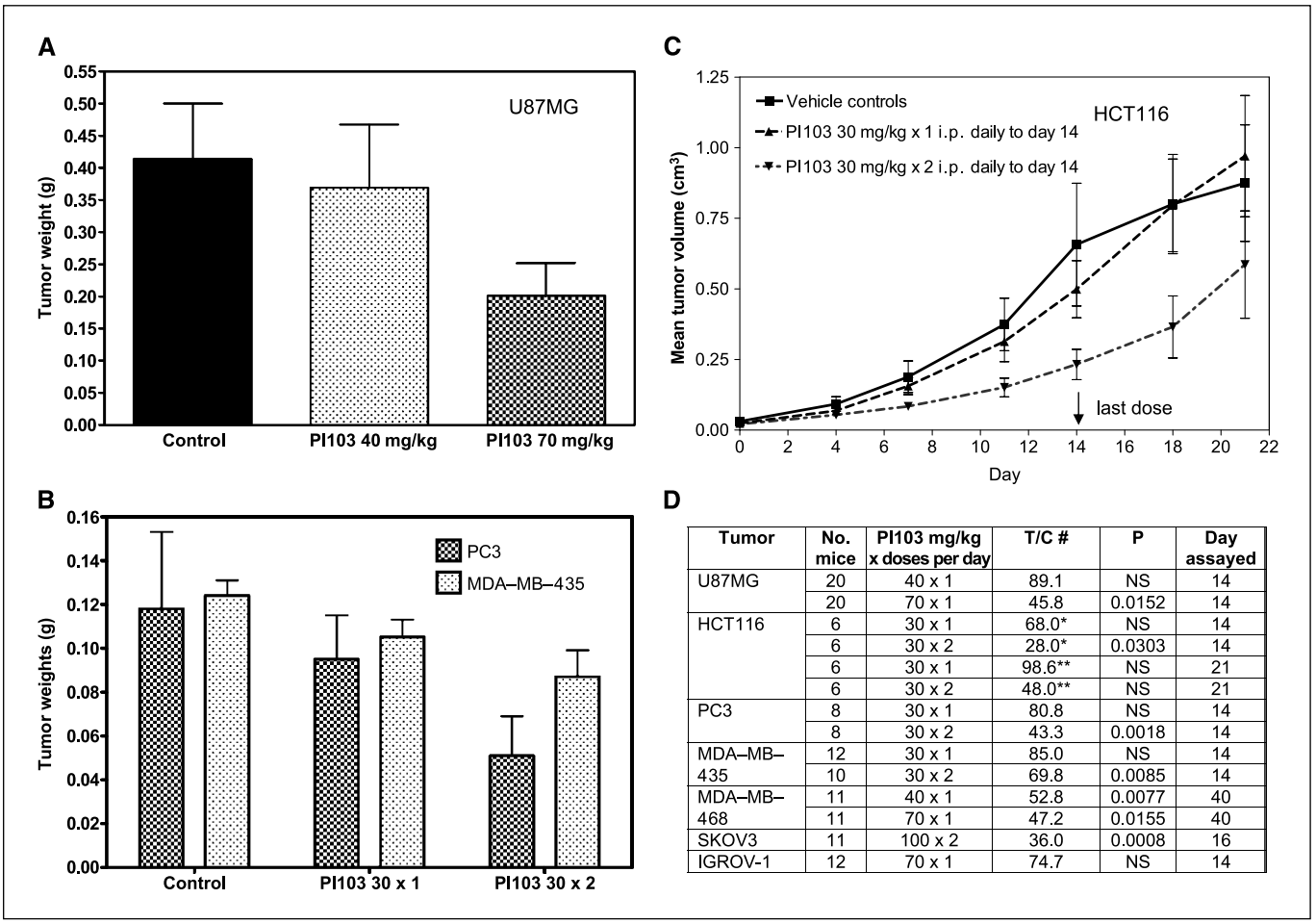

D

Tumor	No. mice	PI103 mg/kg x doses per day	T/C #	P	Day assayed
U87MG	20	40 x 1	89.1	NS	14
	20	70 x 1	45.8	0.0152	14
HCT116	6	30 x 1	68.0*	NS	14
	6	30 x 2	28.0*	0.0303	14
	6	30 x 1	98.6**	NS	21
	6	30 x 2	48.0**	NS	21
PC3	8	30 x 1	80.8	NS	14
	8	30 x 2	43.3	0.0018	14
MDA–MB–435	12	30 x 1	85.0	NS	14
	10	30 x 2	69.8	0.0085	14
MDA–MB–468	11	40 x 1	52.8	0.0077	40
	11	70 x 1	47.2	0.0155	40
SKOV3	11	100 x 2	36.0	0.0008	16
IGROV-1	12	70 x 1	74.7	NS	14

Figure 5. Therapeutic efficacy of PI103 in human tumor xenografts *in vivo. A,* mean final tumor weights of the U87MG human glioma xenografts following dosing with 40 or 70 mg/kg PI103 i.p. daily for 14 d as described in Fig. 4. *B,* mean final tumor weights following dosing with 30 mg/kg PI103 i.p. daily or twice daily or vehicle for 14 d in male mice bearing PC3M prostate carcinomas s.c. (*dark gray columns*) or in female mice bearing MDA-MB-435 breast carcinomas implanted orthotopically in mammary fat pads (*light gray columns*). *C,* mean tumor volumes of HCT116 human colon carcinoma xenografts following dosing with 30 mg/kg PI103 daily or twice daily for 14 d. Tumors were grown in female Ncr athymic mice, and controls received equivalent volumes of vehicle. Note that HCT116 tumors were left to grow out after the end of dosing on day 14. *D,* summary of *in vivo* efficacy of PI103 in a range of human tumor xenografts. #, T/C calculated from tumor weights at termination of the study, except for HCT116. *, calculated from tumor volumes on day 14. **, calculated from tumor volumes on day 21, 7 d after end of therapy.

shown to be frequent in human cancers and result in constitutive activation of the kinase (11). Taken together, these results suggest that PI103 is active in cells exhibiting deregulation of the PI3K pathway by various means, and that several of the oncogenic mutations thus far reported in *PIK3CA* are unlikely to confer resistance to this inhibitor. Further work is required to investigate in more detail the relationship between sensitivity to PI103 and variables such as PI3K mutations/alterations and levels of p-AKT in cancer cells. No obvious relationship is apparent from the present results (Fig. 1*A*). For example, there is a wide range of sensitivity for the cell lines with PTEN abnormalities. However, our studies in an isogenic ovarian cancer model have indicated that a dominant-negative AKT, which shows a decrease in p-AKT Ser ^{473}, is 2-fold less sensitive to PI103 compared with the wild-type cell line.[7]

The cellular potency of PI103 is associated with a decrease in p-AKT Ser ^{473} in all the human cancer cell lines studied as shown here in the U87MG tumor by Western blot analysis and by an electrochemiluminescence immunoassay. This molecular biomarker modulation is consistent with inhibition of the signaling pathway downstream of PI3K and has also been reported recently by others (35). In addition, we were able to show further potent downstream effects on cellular localization of PDK1, AKT1, AKT2, AKT3, and FKHR at concentrations similar to wortmannin in CHO or U20S human osteosarcoma cells stimulated with IGF. In all cell lines examined, treatment with PI103 resulted in a robust growth arrest in the G_1 phase of the cell cycle that was preceded by a decrease in cyclin D1 expression. This is consistent with reports that G_1 cell cycle progression and expression of G_1 cyclins are regulated by PI3K/AKT/mTOR signaling (49) and was also observed in a panel of glioma cell lines (35).

Also of particular interest was our observation that potent and selective inhibition of class I PI3K with PI103 did not result in apoptosis, even at several multiples of the GI_{50} concentrations that

[7] Bhattacharya et al., unpublished data.

clearly resulted in marked inhibition of AKT phosphorylation and complete cytostasis. This lack of apoptosis was exemplified here with HCT116 colon carcinoma tumor cells and was also observed in a wide range of human cancer cell lines tested. It should be noted that the cancer cells used were competent to undergo apoptosis as shown following treatment with LY294002. These data are somewhat surprising given the frequent association of the PI3K pathway with survival signaling and apoptosis (50). However, the expectation of apoptosis upon PI3K inhibition is based heavily on the use of LY294002. In addition to inhibiting other members of the PI3K superfamily and casein kinase 2 (51), it is known that LY294002 induces cell death by producing reactive oxygen species independent of the PI3K pathway in human prostate carcinoma LNCaP cells (52). Interestingly, ZSTK474 was reported as a weak inducer of apoptosis in certain cancer cell lines, an activity more similar to LY294002 than PI103 (30).

In addition to showing potency and selectivity, together with encouraging cytostatic properties in cancer *in vitro*, we wished to show proof of principle for antitumor activity in animal models. To do this, it was necessary to demonstrate that PI103 exhibited suitable pharmacokinetic and pharmacodynamic properties *in vivo*. Although subject to high plasma clearance, PI103 was able to achieve tumor levels above those required for *in vitro* tumor cell growth inhibitory activity for 2 to 4 h with doses of 40 or 70 mg/kg once or twice daily.

PI103 given i.p. at doses of 30 to 100 mg/kg/d showed >50% growth inhibition in a number of human tumor xenograft models selected for deregulation of the PI3K pathway. Significant efficacy was achieved in the PTEN null U87MG glioma, PC3 prostate carcinoma, and MDA-MB-468 breast carcinoma; SKOV-3 ovarian carcinoma and MDA-MB-435 breast carcinoma that overexpress ERB-B2 receptors; and also the SKOV3 ovarian and HCT116 colon carcinoma that express a mutant *PIK3CA*. Fan et al. (34) observed antitumor activity at doses of 5 mg/kg in xenografts derived from U87MG cells transfected with constitutively activated epidermal growth factor receptor (EGFR). We were unable to detect PI103 in

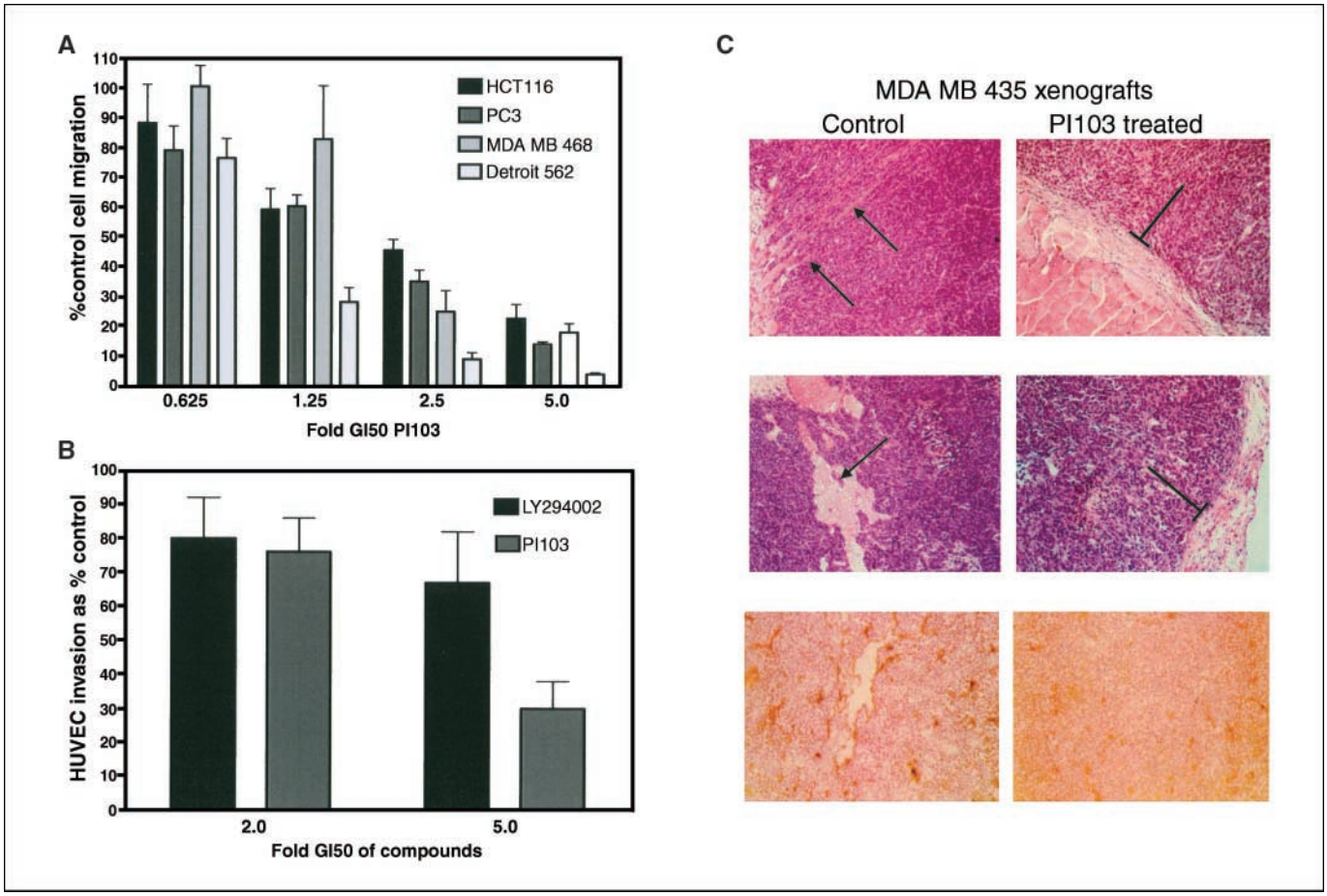

Figure 6. Effects of PI103 on cell migration, invasion, and angiogenesis. *A,* effects of PI103 on tumor cell chemomigration. Cells fluorescently labelled with Celltracker green were seeded into the upper chamber of Fluoroblok filter inserts in 24-well companion plates in DMEM containing vehicle or various concentrations of PI103. Medium containing 5% FCS was placed in the lower chamber as a chemoattractant. The plates were incubated for 16 to 24 h; images were obtained from three fields of view per well; numbers of migrated cells were quantified by digital image analysis. *Columns,* mean (% control values) of three independent experiments; *bars,* SD. HCT116 colon carcinoma (*black columns*), MDA-MB-468 breast carcinoma (*pale gray columns*), PC3 prostate carcinoma (*dark gray columns*), Detroit 562 oropharyngeal carcinoma (*white columns*). *B,* effects of PI103 on HUVEC Matrigel invasion. Cells labeled as above were migrated through a Matrigel barrier towards FCS. Vehicle controls were compared with cells treated with 2× or 5× GI_{50} concentrations of LY294002 or PI103 and invasion scored as above. *C,* effects of PI103 (30 mg/kg twice daily for 14 d) on invasion and angiogenesis of orthotopic MDA-MB-435 breast carcinoma xenografts. Samples were obtained from the same experiment shown in Fig. 5*B*. *Top,* H&E stained to show muscular invasion (*top left*) and vascular invasion (*middle left*) in vehicle-treated tumors (*black arrows*) and well-encapsulated, noninvasive tumors from mice treated with PI103 (*top right* and *middle, black bars*). *Bottom,* tumor sections immunostained with rat anti-mouse endothelial antibody to show the vasculature. Note the extensive, large vessels in control tumor (*bottom left*) compared with small sparse vessels in PI103 treated tumor (*bottom right*).

U87MG xenografts following administration of 5 mg/kg *in vivo* in the same vehicle as used by Fan et al. (50% DMSO in saline), and we saw no down-regulation of p-AKT Ser^{473} by the sensitive electrochemiluminescent immunoassay at that dose (data not shown). However, we observed 89% and 46% T/C following daily treatment of U87MG xenografts with 40 and 70 mg/kg PI103, respectively. This was not surprising given the plasma levels we have observed for PI103. The results suggest that the antitumor activity observed by Fan et al. may be due to the EGFR dependence of the modified U87MG cells used in their study. Those authors also argued, based on the properties of a panel of PI3K inhibitors, that combined activity against p110α and mTOR was important for activity in glioma cell lines. We were able to detect a decrease in AKT phosphorylation *in vivo* in the U87MG glioma tumor and orthotopic OVCAR-3 ovarian carcinoma model both by Western blot and by the more sensitive and quantitative electrochemiluminescent immunoassay. Overall, our *in vivo* antitumor studies show growth inhibition rather than regression in a range of human tumor xenografts with different histologies and molecular pathologies, consistent with the *in vitro* data that indicate a G_1 cell cycle arrest rather than apoptosis.

The antitumor effects were observed at well-tolerated doses, despite the fact that the pharmacokinetic properties of PI103 are suboptimal. This compound is relatively insoluble due to its tricyclic core structure. In addition, it has a number of metabolic hotspots, including the phenol ring, which we have shown is subject to glucuronidation, and the morpholino ring, which is susceptible to hydroxylation. These properties result in high plasma and tissue clearance. We have previously reported similar metabolic hotspots in LY294002 and in NU7026, a DNA-PK inhibitor (47, 48). In particular, it seems that the morpholino ring, which has been reported to bind to the hinge region in PI3Kγ (53–55), is a highly labile moiety and is susceptible to oxidation. Although no significant effect was seen on circulating glucose levels with this agent, and only very limited weight loss was observed (data not shown), it cannot be excluded that a compound with better pharmaceutical properties may be more toxic as well as potentially more effective. Despite the pharmaceutical limitations of PI103, our results show proof of principle for antitumor effects with this class of PI3K inhibitor.

In addition to antiproliferative activity, we showed that PI103 significantly decreased tumor cell chemomigration and invasion. This was seen *in vitro* in four different tumor cell types (including those with mutant *PIK3CA*) and *in vivo* in the MDA-MB-435 breast carcinoma and OVCAR-3 orthotopic ovarian carcinoma model that mimics late-stage clinical disease. The results are consistent with previous studies implicating PI3K in cell motility and invasion (22, 56, 57). The precise isoform(s) involved are still debated and may vary between cell types (57, 58), but PI103 inhibits three class IA PI3K isoforms with equal potency that may contribute to its anti-invasive effects.

Finally, we showed that activated human endothelial cells are also sensitive to PI103, and that greater inhibition of invasion through the Matrigel is obtained compared with LY294002 at equipotent concentrations (based in proliferation GI_{50} values). In addition, we showed that the vascularity of orthotopic MDA-MB-435 breast carcinomas was reduced in PI103-treated mice. Thus, there is a potential for inhibitors of this type to have antitumor activity via effects on angiogenesis as well as through direct action on tumor cells.

In conclusion, we have identified a potent inhibitor of class I PI3K. This compound shows potency *in vitro* and antitumor activity *in vivo* with evidence of target modulation. PI103 represents a valuable tool for exploring the biological functions of class I PI3K enzymes and is a lead for further optimization of this novel class of molecular therapeutics.

Acknowledgments

Received 12/15/2006; revised 3/19/2007; accepted 4/3/2007.

Grant support: Cancer Research UK grants C309/A2187 and C309/A8274.

The costs of publication of this article were defrayed in part by the payment of page charges. This article must therefore be hereby marked *advertisement* in accordance with 18 U.S.C. Section 1734 solely to indicate this fact.

We thank Drs. Khatereh Ahmadi and Yoshitaka Yoneyama for excellent assistance with project management.

References

1. Vanhaesebroeck B, Leevers SJ, Ahmadi K, et al. Synthesis and function of 3-phosphorylated inositol lipids. Annu Rev Biochem 2001;79:535–602.
2. Vanhaesebroeck B, Leevers SJ, Panayotou G, Waterfield MD. Phosphoinositide 3-kinases: a conserved family of signal transducers. Trends Biochem Sci 1997;22:267–72.
3. Rameh LE, Cantley LC. The role of phosphoinositide 3-kinase lipid products in cell function. J Biol Chem 1999;274:8347–50.
4. Cantley LC. The phosphoinositide 3-kinase pathway. Science 2002;296:1655–7.
5. Vanhaesebroeck, B, Ali K, Bilancio A, Geering B, Foukas LC. Signalling by PI 3-Kinase isoforms: insights from gene-targeted mice. Trends Biochem Sci 2005;30: 194–204.
6. Moore SM, Rintoul RC, Walker TR, Chilvers ER, Haslett C, Sethi T. The presence of a constitutively active phosphoinositide 3-kinase in small cell lung cancer cells mediates anchorage-independent proliferation via a protein kinase B and p70S6k-dependent pathway. Cancer Res 1998;58:5239–47.
7. Shaw RJ, Cantley LC. Ras, PI(3)K and mTOR signalling controls tumour cell growth. Nature 2006;441:424–30.
8. Shayesteh L, Lu Y, Kuo WL, et al. PIK3CA is implicated as an oncogene in ovarian cancer. Nat Genet 1999;21: 99–102.
9. Rogers S, Box C, Harrington K, Rhys-Evans P, Eccles S. The phosphoinositide 3-kinase signalling pathway as a therapeutic target in head and neck squamous cell carcinoma. Expert Opin Ther Targets 2005;9:769–90.
10. Vivanco I, Sawyers CL. The phosphatidylinositol 3-kinase AKT pathway in human cancer. Nat Rev Cancer 2002;2:489–501.
11. Samuels Y, Wang Z, Bardelli A, et al. High frequency of mutations of the PIK3CA gene in human cancers. Science 2004;304:554.
12. Samuels Y, Diaz LA, Schmidt-Kittler O, et al. (2005) Mutant PIK3CA promotes cell growth and invasion of human cancer cells. Cancer Cell 2005;7:561–73.
13. Broderick DK, Di C, Parrett TJ, et al. Mutations of PIK3CA in anaplastic oligodendrogliomas, high-grade astrocytomas and medulloblastomas. Cancer Res 2004; 64:5048–50.
14. Kang S, Bader AG, Vogt PK. Phosphatidylinositol 3-kinase mutations identified in human cancer are oncogenic. Proc Natl Acad Sci U S A 2005;102:802–7.
15. Kang S, Denley A, Vanhaesebroeck B, Vogt PK. Oncogenic transformation induced by the p110beta, -gamma, and -delta isoforms of class I phosphoinositide 3-kinase. Proc Natl Acad Sci U S A 2006;103:1289–94.
16. Sulis ML, Parsons R. PTEN: from pathology to biology. Trends Cell Biol 2003;13:478–83.
17. Nakatani K, Thompson DA, Barthel A, et al. Up-regulation of Akt3 in estrogen receptor-deficient breast cancers and androgen-independent prostate cancer lines. J Biol Chem 1999;274:21528–32.
18. Li Q, Zhu GD, Kokubo Y, et al. Targeting Serine/threonine protein kinase B/Akt and cell-cycle checkpoint kinases for treating cancer. Curr Top Med Chem 2002;2:939–71.
19. Findlay GM, Harrington LS, Lamb RF. TSC1–2 tumour suppressor and regulation of mTOR signalling: linking cell growth and proliferation. Curr Opin Genet Dev 2005;15:69–76.
20. Bell HS, Ryan KM. Intracellular signalling and cancer: complex pathways lead to multiple targets. Eur J Cancer 2005;41:206–15.
21. Jimenez C, Portela RA, Mellado M. Role of the PI 3-Kinase regulatory subunit in the control of actin organization and cell migration. J Cell Biol 2000;151:249–62.
22. Brader S, Eccles SA. Phosphoinositide 3′ kinase signalling pathways in tumour progression, invasion and angiogenesis. Tumori 2004;90:2–8.
23. Shien T, Doihara H, Hara H, et al. PLC and PI 3-Kinase pathways are important in the inhibition of EGF-induced cell migration by gefitinib ('Iressa', ZD1839). Breast Cancer 2004;11:367–73.
24. Maffucci T, Cooke FT, Foster FM, Traer CJ, Fry MJ, Falasca M. Class II phosphoinositide 3-kinase defines a novel signalling pathway in cell migration. J Cell Biol 2005;169:789–99.
25. Workman P. Inhibiting the phosphoinositide 3-kinase pathway for cancer treatment. Biochem Soc Trans 2004;32:393–6.
26. Drees BE, Mills GB, Rommel C, Prestwich GD. Therapeutic potential of phosphoinositide 3-kinase inhibitors. In: Expert Opin Ther 2004 Patents. Ashley Publications. 14:703–25.

27. Yu K, Lucas J, Zhu T, et al. PWT-458, A novel pegylated-17-hydroxywortmannin, Inhibits phosphatidylinositol 3-kinase signaling and suppresses growth of solid tumours. Cancer Biol Ther 2005;4: 538–45.

28. Ihle NT, Williams R, Chow S, et al. Molecular pharmacology and antitumour activity of PX-866, a novel inhibitor of phosphoinositide-3-kinase signaling. Mol Cancer Ther 2004;3:763–72.

29. Ihle NT, Paine-Murrieta G, Berggren MI, et al. The phosphatidylinositol-3-kinase inhibitor PX-866 overcomes resistance to the epidermal growth factor receptor inhibitor gefitinib in A-549 human non-small cell lung cancer xenografts. Mol Cancer Ther 2005;9: 1349–57.

30. Yaguchi S, Fukui Y, Koshimizu I, et al. Antitumour activity of ZSTK474, a new phosphatidylinositol 3-kinase inhibitor. J Natl Cancer Inst 2006;98:545–56.

31. Hayakawa M, Kaizawa H, Moritomo H, et al. Synthesis and biological evaluation of 4-morpholino-2-phenylquinazolines and related derivatives as novel PI3 kinase p110alpha inhibitors. Bioorg Med Chem 2006;14: 6847–58.

32. Hayakawa M, Kaizawa H, Moritomo H, et al. Synthesis and biological evaluation of pyrido[3′,2′:4,5]furo[3,2-d]pyrimidine derivatives as novel PI3 kinase p110alpha inhibitors. Bioorg Med Chem Lett 2007;17:2438–42. Epub ahead of print 2007 Feb 15.

33. Hayakawa M, Kaizawa H, Moritomo H, et al. Synthesis and biological evaluation of pyrido[3′,2′:4,5]furo[3,2-d]pyrimidine derivatives as novel PI3 kinase p110alpha inhibitors. Bioorg Med Chem Lett 2007;1: 2438–42.

34. Knight ZA, Gonzalez B, Feldman ME, et al. A pharmacological map of the PI3-K family defines a role for p110alpha in insulin signaling. Cell 2006;125: 733–47.

35. Fan QW, Knight ZA, Goldenberg DD, et al. A dual PI3 kinase/mTOR inhibitor reveals emergent efficacy in glioma. Cancer Cell 2006;9:341–9.

36. Workman P, Clarke PA, Guillard S, Raynaud FI. Drugging the PI3 kinome. Nat Biotechnol 2006;24:794–6.

37. Holford J, Sharp SY, Murrer BA, Abrams M, Kelland LR. *In vitro* circumvention of cisplatin resistance by the novel sterically hindered platinum complex AMD473. Br J Cancer 1998;77:366–73.

38. Smith NF, Hayes A, Nutley BP, Raynaud FI, Workman P. Evaluation of the cassette dosing approach for assessing the pharmacokinetics of geldanamycin analogues in mice. Cancer Chemother Pharmacol 2004;54:475–86.

39. Workman P, Balmain A, Hickman JA. United Kingdom Co-ordinating Committee on Cancer Research (UKCCR) guidelines for the welfare of animals in experimental neoplasia. Second edition UKCCR. Br J Cancer 1997;77:1–10.

40. Gabrielsson J, Weiner D. Pharmacokinetic and pharmacodynamic data analysis, concepts and applications, 1997 3rd ed. Stockholm (Sweden): Swedish Pharmaceutical Press; ISBN 91-8627-492-9.

41. Eccles SA, Court WJ, Box GA, Dean CJ, Melton RG, Springer CJ. Regression of established breast carcinoma xenografts with antibody-directed enzyme prodrug therapy against c-erbB2 p185. Cancer Res 1994;54: 5171–7.

42. Sanderson S, Valenti M, Gowan S, et al. Benzoquinone ansamycin heat shock protein 90 inhibitors modulate multiple functions required for tumor angiogenesis. Mol Cancer Ther 2006;5:522–32.

43. Shingu T, Yamada K, Hara N, et al. Growth inhibition of human malignant glioma cells induced by the PI3-K-specific inhibitor. J Neurosurg 2003;98:154–61.

44. Lu Y, Lin YZ, LaPushin R, et al. The PTEN/MMAC1/TEP tumour suppressor gene decreases cell growth and induces apoptosis and anoikis in breast cancer cells. Oncogene 1999;18:7034–45.

45. Brazil DP, Hemmings BA. Ten years of protein kinase B signalling: a hard Akt to follow. Trends Biochem Sci 2001;26:657–64.

46. Brunet A, Bonni A, Zigmond MJ, et al. Akt promotes cell survival by phosphorylating and inhibiting a Forkhead transcription factor. Cell 1999;96:857–68.

47. Nutley BP, Raynaud FI, Hayes A, Goddard P, Jarman M, Workman P. (2001). Pharmacokinetics and metabolism of the phosphatidylinositol-3 kinase inhibitor LY294002 in the mouse. Proc Am Assoc Cancer Res 2001;42:2044.

48. Nutley BP, Smith NF, Hayes A, et al. Pharmacokinetics and metabolism of a novel DNA-PK inhibitor NU7026. Br J Cancer 2005;93:1011–8.

49. Gao N, Flynn DC, Zhang Z, et al. G1 cell cycle progression and the expression of G_1 cyclins are regulated by PI 3-Kinase/AKT/mTOR/p70S6K1 signaling in human ovarian cancer cells. Am J Physiol Cell Physiol 2004;287:C281–91.

50. Erhardt P, Cooper GM. Activation of the CPP32 apoptotic protease by distinct signaling pathways with differential sensitivity to Bcl-xL. J Biol Chem 1996;271: 17601–4.

51. Davies SP, Reddy H, Caivano M, Cohen P. Specificity and mechanism of action of some commonly used protein kinase inhibitors. Biochem J 2000;351:95–105.

52. Poh TW, Pervaiz S. LY294002 and LY303511 sensitize tumor cells to drug-induced apoptosis via intracellular hydrogen peroxide production independent of the phosphoinositide3-kinase-Akt pathway. Cancer Res 2005;65:6264–74.

53. Walker EH, Pacold ME, Perisic O, et al. Structural determinants of phosphoinositide 3-kinase inhibition by wortmannin, LY294002, quercetin, myricetin, and staurosporine. Mol Cell 2000;6:909–19.

54. Walker EH, Perisic O, Ried C, Stephens L, Williams RL. Structural insights into phosphoinositide 3-kinase catalysis and signalling. Nature 1999;402:313–20.

55. Pacold ME, Suire S, Perisic O, et al. Crystal structure and functional analysis of Ras binding to its effector phosphoinositide 3-kinase gamma. Cell 2000;103:931–43.

56. Jones GE, Prigmore E, Calvez R, et al. Requirement for PI 3-Kinase gamma in macrophage migration to MCP-1 and CSF-1. Exp Cell Res 2003;290:20–31.

57. Kaufmann J, Pronk G, Giese K, Klippel A. Identification of novel effectors of invasive growth downstream of phosphoinositide 3-kinase. Biochem Soc Trans 2004;32: 355–9.

58. Sawyers CL. Opportunities and challenges in the development of kinase inhibitor therapy for cancer. Genes Dev 2003;17:2998–3010.